Polarization dependence of the nonlinear optical responses of $KTa_{1-x}Nb_xO_3$ crystals after picosecond-pulse laser excitation

Huimin Liu,* Roger J. Reeves,† and Richard C. Powell‡
Center for Laser Research, Oklahoma State University, Stillwater, Oklahoma 74078

L. A. Boatner
Solid State Division, Oak Ridge National Laboratory, Oak Ridge, Tennessee 37830

(Received 12 October 1993)

Fast nonlinear optical signals on picosecond and nanosecond time scales have been studied in the mixed crystal system $KTa_{1-x}Nb_xO_3$ using transient degenerate four-wave mixing. The two distinct signal components, denoted as an instantaneous response and slow response in previous studies, show the dependence of the polarization configuration of the optical pulses. The results were consistent with a lattice-relaxation model based on the laser-induced dynamic displacement of the Nb ion. In this model the signal variations result from the competition between the dynamic displacement and the intrinsic distortion associated with the spontaneous polarization along the optic axis.

I. INTRODUCTION

The mixed crystal system of $KTa_{1-x}Nb_xO_3$ (KTN) is of particular interest among perovskite-structure ABO_3 materials[1-3] because at room temperature it undergoes a phase transition as the niobium concentration x increases from O ($KTaO_3$) to 1 ($KNbO_3$). In recent years research has been focused on understanding the mechanism responsible for these structural changes.[4-7] A recently suggested model predicts relaxation modes in which the B ions (Nb or Ta) move from one equilibrium site to another in the multiwell potential.[6]

In order to enhance the understanding of these polar ion hopping modes and other fast physical processes in these materials, we have initiated degenerate four-wave mixing (DFWM) studies of KTN crystals using a picosecond laser excitation source. Previous results showed that there were two distinctly different contributions to the FWM signal in the temporal range of picoseconds to nanoseconds.[8-10] The first was an instantaneous response (IR) signal with a time width of ~ 30 ps, which is close to the cross-correlation width of the two write-beam pulses. It was suggested that this signal was associated with contributions from bound charges, free carriers, and stimulated scattering from the polar hopping modes of the Nb^{5+} ions.[8]

The second contribution of the FWM signal was a slow response (SR) that had a rise time of about a hundred picoseconds and a decay time of several nanoseconds. A lattice relaxation model was developed that attributed the SR signal to a population grating produced when free carriers were trapped on Nb^{5+} ions to produce excited Nb^{4+} ions.[9,10] This excitation migrates among the niobium ions as a small polaron for several nanoseconds until it decays at defect sites. In this model the temporary dynamic disorder caused by the laser excitation is added to the local static disorder of the lattice,[5] and the intrinsic distortion of the central B ion along the polar axis direction can be associated with the niobium concentration via crystallographic data. It was found that the theoretical predictions of this model are in good agreement with the experimental results.

In this work we describe the results of further measurements of the picosecond DFWM signals in KTN crystals. The experimental setup has been depicted in Refs. 9,10. The results obtained in this work support the models proposed previously to explain the IR and SR components of the nonlinear optical signal.

II. POLARIZATION DEPENDENCE OF THE DFWM SIGNALS

The two write-beam pulses and the probe pulse were set independently to either s or p polarization directions. The signals were detected with the same polarization direction as that of the probe pulse. We use the convention (*ssp*) to denote the polarizations of the write beams A,B (s polarized), and the probe beam (p polarized). All of the samples were oriented such that the grating vector was parallel either to their cubic axes or to orthorhombic-phase principal axes. Figure 1 shows the relative DFWM signal intensities for the different polarization combinations in the undoped cubic $KTaO_3$.

A. Parallel polarizations

The two write beams A and B intersect at an angle of 2θ inside the sample and the grating vector $\mathbf{q}=\pm(\mathbf{k}_A-\mathbf{k}_B)$. The electric field amplitude A along the x direction is[11]

$$\mathbf{A}=\mathbf{A}_A e^{+ik_x x}+\mathbf{A}_B e^{-ik_x x}, \tag{1}$$

where k_x is the magnitude of the x component of the write-beam wave vector. The light intensity along the x axis is then

$$I=I_A+I_B+2\Delta I\cos(2k_x x), \tag{2}$$

where $\Delta I=1/2n\epsilon_0\mathbf{A}_A\cdot\mathbf{A}_B$. For identical polarizations of A_A and A_B, and $I_A=I_B$, $I=2I_A[1+\cos(qx)]$ for polarizations (*ss*), and $I=2I_A+nc\epsilon_0|A_{Ax}A_{Bx}^*+A_{Az}A_{Bz}^*|\cos(qx)$ for polarizations (*pp*). Thus the light intensity of the interference pattern is modulated along the x axis, and therefore the charge-carrier density and Nb^{4+} distributions that are produced are also modulated along the x axis.

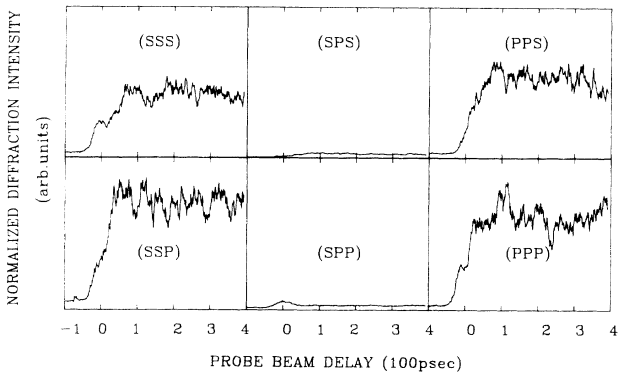

FIG. 1. Relative diffraction intensity versus probe-pulse delay for different laser polarization configurations.

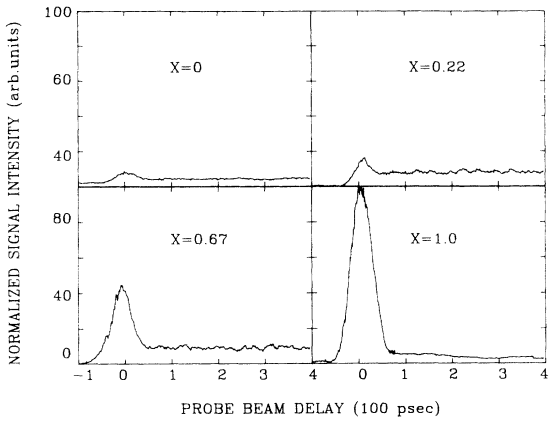

FIG. 2. Relative diffraction intensity vs probe-pulse delay as a function of niobium concentration in (*spp*) configuration.

When the two write-beam pulses are polarized in the same direction, the IR signal component is directly related to the third order susceptibility by[12,13]

$$\eta = \exp(-\alpha d/\cos\theta)\sin^2(d\pi\Delta n/\lambda\cos\theta) , \quad (3)$$

where $\Delta n(12\pi/n_0\langle E^2\rangle)\chi^{(3)}$. Comparing the polarization configuration (*sss*) to (*ppp*) shows that $\chi_{ssss}=\chi_{pppp}$ or $\chi_{iiii}=\chi_{jjjj}$ due to the cubic symmetry. χ_{spps} and χ_{pssp} are independent. From the absolute DFWM diffraction-efficiency measurements the following parameters were obtained for the cubic $KTaO_3$ crystal: $\chi^{(3)}_{1111}=\chi^{(3)}_{2222}=\chi^{(3)}_{3333}=0.32\times10^{-13}$; $\chi^{(3)}_{1221}=0.51\times10^{-13}$; $\chi^{(3)}_{2112}=0.43\times10^{-13}$ cm^3 erg. Similar polarization-dependence studies on other KTN crystals with different niobium concentrations were also carried out. Some of the important results are:

(1) In the (*pps*) and (*ppp*) configurations the IR signal intensity decreases with increasing Nb concentration, but is enhanced for $KNbO_3$. However, the SR signal intensity decreases monotonically with increasing niobium concentration for all values of x. In these configurations, the superposition of the two write pulses results in an elliptic instead of a linear polarization. The probe beam senses the grating that is established through the third-order susceptibility with its various symmetry components for the $KTa_{1-x}Nb_xO_3$ crystals.

(2) In the (*sss*) and (*ssp*) configurations the IR and SR signal intensities exhibit anomalous behavior approaching the region of $x\sim0.3$, which corresponds to the phase transition at room temperature. This behavior of the SR signal was studied in Refs. 9 and 10 and was found to be due to lattice relaxation associated with a population grating of excited Nb^{4+} ions. The concentration dependence of the IR signal is a new result and is discussed in detail in Sec. III.

B. Orthogonal polarizations

For the mixed polarization configurations (*sp*) or (*ps*), the optical electric fields of the two write beams are perpendicular to each other and $\Delta I=0$. Thus there is no intensity modulation inside the sample and no scalar grating is produced. The bound-charge contribution to the IR signal and the lattice-relaxation contribution to the SR signal are therefore negligible in the mixed polarization configurations. The DFWM results in Fig. 1 for (*sps*) and (*spp*) configurations show that no distinct signals can be observed in these configurations in $KTaO_3$. However, as the niobium concentration was increased, an enhancement of the intensity of the IR component was observed in the (*spp*) configuration. These configurations are associated with impulsive driving of Nb hopping modes and strong signals are observed from $KNbO_3$ crystals under these conditions.[7]

Figure 2 shows transients recorded for four Nb concentrations with the maximum intensity occurring in $KNbO_3$ ($x=1$). It was found that the diffracted signal had both p- and s-polarization components although the probe pulse was only p polarized. In our counterpropagating pump-beam geometry,[9] part of the s-polarized component may be due to the phase-conjugated A write beam or to the linearly polarized probe beam interacting with the circular polarization-type grating. However because of the strong Nb concentration dependence it is most likely that the increasing signal arises from a particular Nb ion hopping mode.

As pointed out by Sokoloff, Chase, and Rytz the laser-induced dynamic disorder in $KNbO_3$ crystals has directional properties. In particular, there is disorder along the c axis designated as an A_1-symmetry mode and disorder in the ab plane designated as a (B_1+B_2)-symmetry mode. The polarization configuration of (*sp*) for the two write beams and crystal geometry of $K_g\|c$ is the appropriate arrangement for the impulsive driving of the Nb ion hopping mode of B_2 symmetry. Our results clearly show the onset of scattering intensity from this process with increasing Nb concentration.

III. DEPENDENCE OF THE DFWM SIGNAL IN THE VICINITY OF A PHASE TRANSITION

In (*ssp*) configuration the SR component of the signal is intense with a rise time of a few tens of picoseconds, and the IR component appears suppressed by the SR component. As discussed in Refs. 9 and 10, the absolute DFWM diffraction efficiency increases, and reaches a maximum when the niobium concentration goes from $x=0$ to near $x\sim0.3$, which corresponds to a phase transition at room temperature. This anomalous concentration dependence has been recognized as a result of the

competition between the local dynamic distortion induced by the laser and the static distortion of the lattice. In the (*sss*) configuration however, the diffraction efficiency of the observed IR signal intensity versus x also exhibits a maximum in the vicinity of $x \sim 0.3$. As shown in Fig. 3 the data are the measured absolute DFWM diffraction efficiencies for the IR and SR signals normalized to the same grating thickness.

The similar functional dependences of the IR and SR components with concentration shown in Fig. 3 suggest that the dynamic distortion model used in Ref. 10 for the SR signal can be used to understand the IR signal. The amplitude of the dynamic distortion of the SR signal was assumed to be a linear function of niobium concentration: $\Delta = \beta_3 x$. In this case the linear coefficient was uniquely determined from luminescence measurements.[10]

There is no such direct observation of the amplitude of the dynamic distortions behind the IR signal component. However, laser-induced-phonon spectroscopy (LIPS)[14,15] can provide information about the dynamic displacements of the related force constants. The LIPS signal is generated from density fluctuations caused by the interaction of the optical electric field with the acoustic field of the crystal. Our interpretation is that the functional dependence of the LIPS signal with niobium concentration can be used to describe the dependence of the dynamic distortion associated with the IR signal.

Figure 4 shows the LIPS spectra of $KTa_{1-x}Nb_xO_3$ crystals with different niobium concentrations. The signal in the nanosecond range represents the superposition of the SR signal component and the LIPS signal. Knowing the absolute value of the SR component allows the LIPS signal amplitude to be extracted. The observed

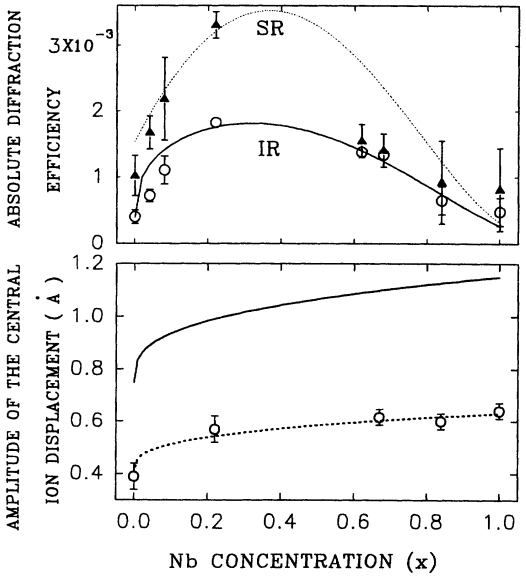

FIG. 3. Absolute diffraction efficiencies of IR and SR signal intensities (top), and the amplitude of the central B ion displacement (bottom) as a function of niobium concentration x. The data point represent the experimental values while the curves represent the theoretical fit. The solid line of the bottom graph shows the dynamic part of the B ion displacement associated with the IR signal in DFWM.

diffraction efficiency in the LIPS measurements is described by[14]

$$\eta = \left[\pi \rho \frac{\delta n}{\delta \rho} \frac{\Delta S d}{\lambda \cos\phi} \right]^2 , \tag{4}$$

where ρ is the density, and the acoustic response S is given by

$$S = -C \cos(ky) \sin(\omega t) , \tag{5}$$

where C is the amplitude of the acoustic wave, k is the grating vector, and ω is the acoustic frequency.

The amplitudes of the displacement associated with the LIPS signal were extracted from the data for each niobium concentration and are shown as the data points in Fig. 3 (bottom panel). These data were fit to a general equation of the form

$$C = A_{KTaO_3} + A_1 x^{A_2} , \tag{6}$$

where A_{KTaO_3}, A_1, and A_2 are parameters and x is the niobium concentration. The best fit is shown as the dashed line in Fig. 3 (bottom panel) and was obtained with the parameters $A_{KTaO_3} = 0.41$ Å, $A_1 = 0.22$ Å, $A_2 = \frac{1}{3}$.

Having established the functional form given in Eq. (6) for the dynamic displacement, we can use the expression derived previously for the DFWM diffraction efficiency as a function of niobium concentration:[10]

$$\eta_{max} = f(\theta, \xi, \lambda, n, d, I, dt)(r_{KTaO_3} + \beta_1 x)^4 \times (B_{KTaO_3} + \beta_3 x^{1/3} - \beta_2 x)^2 . \tag{7}$$

This expression was used to fit the data in Fig. 3 using the values of r_{KTaO_3}, β_1, and β_2 derived previously. The parameters B_{KTaO_3}, β_3 and $f(\theta, \xi, \lambda, n, d, I, dt)$ were allowed to vary, but the ratio between B_{KTaO_3} and β_3 remained fixed at the value determined by the results of the LIPS data. The results of the fit are shown as the solid line in

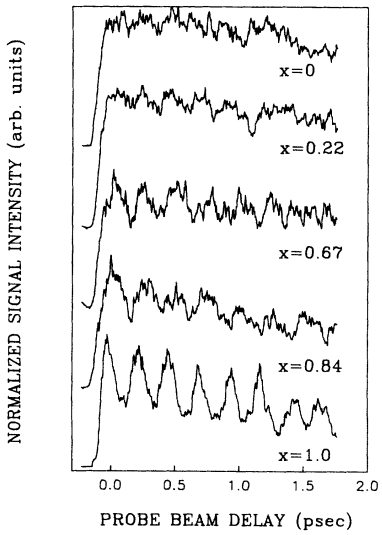

FIG. 4. Laser-induced-phonon spectroscopy (LIPS) of $KTa_{1-x}Nb_xO_3$ crystals with different niobium concentrations. The experiment was conducted in the (*ssp*) configuration.

Fig. 3 and as can be seen the agreement is satisfactory given that restrictions were placed on some parameters. The values of all the parameters used in this fit are: $f(q,x,l,n,d,I,dt)=0.12\times10^{-3}$, $r_{KTaO_3}=1.99$ Å, $\beta_1=0.86$ Å, $\beta_2=0.88$ Å, $\beta_3=0.40$ Å, $B_{KTaO_3}=0.75$ Å. In Fig. 3 the amplitude of the displacement from the IR signal, as represented by the function $B_{KTaO_3}+\beta_3 x^{1/3}$, is plotted as the solid line of the lower graph.

IV. INSTANTANEOUS RESPONSE SIGNAL COMPRESSION

At low intensity the signal maximum occurs at $t=0$, i.e., when the probe pulse is arriving at the sample at exactly the same time as the two pump pulses. However, at high laser fluences the IR signal peak is observed at negative probe-delay times and the temporal width shortens to be less than the cross-correlation time. Figure 5 shows a DFWM transient in the polar $KNbO_3$ sample compared to that recorded from the CS_2. Note that the laser intensity used here is considerably higher than the intensities discussed in the earlier figures.

In order to understand the mechanisms producing these changes, the intensity of the transmitted probe beam was recorded as a function of probe-beam delay with only one pump beam incident on the sample (see the bottom panel of Fig. 5). As this figure shows, the amount of light reaching the detector is not constant, and the probe beam suffers considerable attenuation when it arrives in the sample in conjunction with the strong pump beam. This loss of intensity indicates that there is a two-photon absorption (TPA) interaction between the pump and probe beams. Note that the intensity does not return to its initial level when the probe is delayed longer.

These signals are interpreted in the following manner. At negative delay times the detected signal represents the undisturbed probe intensity. As the probe is delayed in time it begins to interact with the pump pulse and two-photon absorption decreases the transmitted intensity. The attenuation rises with the cross-correlation time of the optical pulses since TPA is an instantaneous process. The two-photon excitation produces free carriers in the conduction band and the attenuation decreases with the free-carrier lifetime of about 100 ps. Note that the same time scale was observed in the DFWM experiments for the free-carrier lifetime. The mechanism of free-carrier relaxation is trapping at Nb^{5+} ion sites to produce Nb^{4+}. Thus, the long-lived attenuation is interpreted as absorption due to the production of Nb^{4+} ions.

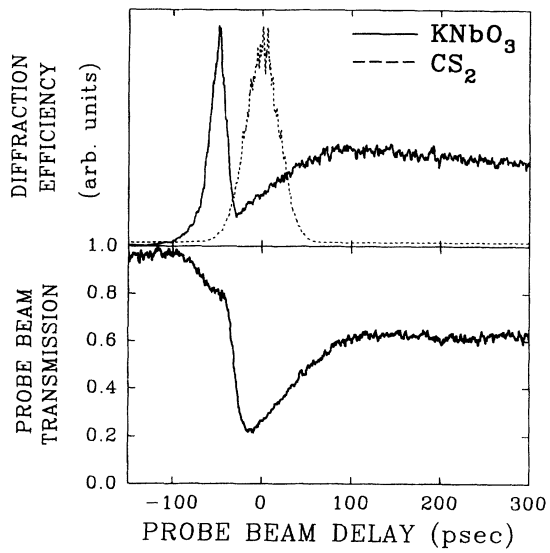

FIG. 5. Transient DFWM signal from a $KNbO_3$ crystal. Top panel: with a lower fluence of 280 mJ/cm^2 showing the shift in the IR signal peak. The polarization configuration was (*sss*) and the crystal was aligned with $K_g \| c$ axis. Bottom panel: the intensity of the probe beam transmitted through a $KNbO_3$ crystal as a function of the delay time.

As the probe pulse moves into coincidence with the pump pulses, the two-photon excitation between any two pulses in the experiment acts to decrease the amount of light reaching the detector. What makes the effect particularly apparent is that the TPA process is of higher order and thus is expected to be more pronounced at high intensities. Thus the recorded DFWM signal looks like the sum of a positive signal centered at $t=0$ and a higher-order negative signal, which gives a shift of its maximum signal to negative delay times and a narrowing of the temporal width.

*Present address: Department of Physics, University of Puerto Rico, Mayaguez, Puerto Rico 00680.
†Present address: Department of Physics & Astronomy, University of Canterbury, Christchurch, New Zealand.
‡Present address: Optical Sciences Center, University of Arizona, Tucson, AZ 85721.

[1]W. Kleeman, F. J. Schafer, and D. Rytz, Phys. Rev. Lett. **54**, 2038 (1985).
[2]J. Toulouse, X. M. Wong, and L. A. Boatner, Solid State Commun. **68**, 353 (1988).
[3]J. P. Sokoloff, L. L. Chase, and L. A. Boatner, Phys. Rev. B **41**, 2398 (1990).
[4]J. Grenier, D. Houde, S. Jande, and L. A. Boatner, Phys. Rev. B **47**, 1 (1993).
[5]J. P. Sokoloff, L. L. Chase, and D. Rytz, Phys. Rev. B **38**, 597 (1988).
[6]R. Comes, M. Lambert, and A. Gruinier, Solid State Commun. **6**, 715 (1968).
[7]T. P. Dougherty, G. P. Wiederrecht, and K. A. Nelson, Ferroelectrics **120**, 79 (1991).
[8]R. J. Reeves, M. J. Jani, B. Jassemnejad, R. C. Powell, G. J. Mizell, and W. Fay, Phys. Rev. B **43**, 71 (1991).
[9]H. Liu, R. C. Powell, and L. A. Boatner, J. Appl. Phys. **70**, 20 (1991).
[10]H. Liu, R. C. Powell, and L. A. Boatner, Phys. Rev. B **44**, 2461 (1991).
[11]*Laser-induced Dynamic Gratings,* edited by H. J. Eichler, P. Gunter, and D. W. Pohl, Springer Series in Optical Sciences Vol. 50 (Springer Verlag, Berlin, 1986).
[12]H. Kogelink, Bull. Syst. Technol. J. **48**, 2909 (1969).
[13]*CRC Handbook of Laser Science and Technology,* edited by M. J. Weber (CRC Press, Boca Raton, 1985), Vol. III, p. 263.
[14]K. A. Nelson, D. R. Lutz, M. D. Fayer, and L. Madison, Phys. Rev. B **24**, 3261 (1981).
[15]K. A. Nelson, J. Appl. Phys. **53**, 6060 (1982).